INORGANIC CHEMISTRY
FRONTIERS

RESEARCH ARTICLE

View Article Online
View Journal | View Issue

Cite this: *Inorg. Chem. Front.*, 2023, **10**, 2754

Accelerated rates of proton coupled electron transfer to oxygen deficient polyoxovanadate–alkoxide clusters†

Shannon E. Cooney, ‡ Eric Schreiber, ‡ William W. Brennessel and Ellen M. Matson *

Received 19th January 2023,
Accepted 3rd April 2023

DOI: 10.1039/d3qi00129f

rsc.li/frontiers-inorganic

Anionic dopants, such as O-atom vacancies, alter the thermochemical and kinetic parameters of proton coupled electron transfer (PCET) at metal oxide surfaces; understanding their impact(s) is essential for informed material design for efficient energy conversion processes. To circumvent challenges associated with studying extended solids, we employ polyoxovanadate–alkoxide clusters as atomically precise models of reducible metal oxide surfaces. In this work, we examine net hydrogen atom (H-atom) uptake to an oxygen deficient vanadium oxide assembly, $[V_6O_6(MeCN)(OCH_3)_{12}]^0$. Addition of two H-atom equivalents to $[V_6O_6(MeCN)(OCH_3)_{12}]^0$ results in formation of $[V_6O_5(MeCN)(OH_2)(OCH_3)_{12}]^0$. Assessment of the bond dissociation free energy of the O–H bonds of the resultant aquo moiety reveals that the presence of an O-atom defect weakens the O–H bond strength. Despite a decreased thermodynamic driving force for the reduction of $[V_6O_6(MeCN)(OCH_3)_{12}]^0$, kinetic investigations show the rate of H-atom uptake at the cluster surface is ~100× faster than its oxidized congener, $[V_6O_7(OCH_3)_{12}]^0$. Electron density derived from the O-atom vacancy is shown to play an important role in influencing H-atom uptake at the cluster surface, lowering activation barriers for H-atom transfer.

Introduction

The last several decades have seen significant advances in renewable energy technologies,[1] driving rapid, global adoption of low-carbon electricity.[2,3] However, continued progress toward a sustainable energy economy requires a transition from our dependence on fossil fuels. Electrochemistry can play a key role, namely through the development of electrochemical catalysts that recycle low-value precursors into chemical fuels.[4] In the context of electrosynthetic hydrogenations, the concerted transfer of protons and electrons (*i.e.* proton coupled electron transfer, PCET) can uniquely enable the activation of energy-poor substrates by bypassing intermediates.[5,6] While proton and electron transfer at metal oxides have been studied extensively in the field of electrochemical energy storage,[7,8] researchers have only recently started to understand these processes in the presence of substrate.[9,10] As such, further progress in the effective use of these materials as hydrogenation catalysts requires atomistic understanding of surface-mediated PCET reaction mechanisms.

In materials science, O-atom deficiencies are considered a form of anionic dopant (Fig. 1). Their presence increases carrier density within a material, as the lack of an oxide ligand necessitates the presence of a reduced metal center.[10,11] Accordingly, the Fermi energy of materials possessing O-atom defects is often disparate from that of their oxidized congeners; increased electron density in the extended solid modifies the driving force of electron transfer.[12] This change in effective reduction potential of the material has been demonstrated *via* theoretical calculations to result in dramatic differences in bond dissociation free energies, BDFE(O–H), of surface hydroxide moieties in these materials.[13]

Our research team is interested in understanding factors that influence PCET reactivity that yields net hydrogen atom (H-atom) uptake at the surface of a series of vanadium oxide assemblies.[14–20] The polyoxovanadate–alkoxide (POV–alkoxide) clusters studied by our team possess bridging *alkoxide* ligands, blocking traditionally nucleophilic sites at the surface of molecular metal oxide assemblies that dictate their reactivity with protons in solution.[20–28] In some cases, saturation of bridging sites by organic groups has been studied as a means to isolate

Department of Chemistry, University of Rochester, Rochester, NY 14627, USA. E-mail: matson@chem.rochester.edu

†Electronic supplementary information (ESI) available: ^{1}H NMR of complexes and reactions, X-ray crystal structure parameters, bond-valence sum calculations, and electronic absorption spectrum of $[V_6O_6(OH_2)]^0$, and kinetic analyses for the reduction of $[V_6O_6(MeCN)]^0$. CCDC 2234804. For ESI and crystallographic data in CIF or other electronic format see DOI: https://doi.org/10.1039/d3qi00129f

‡These authors contributed equally to this work.

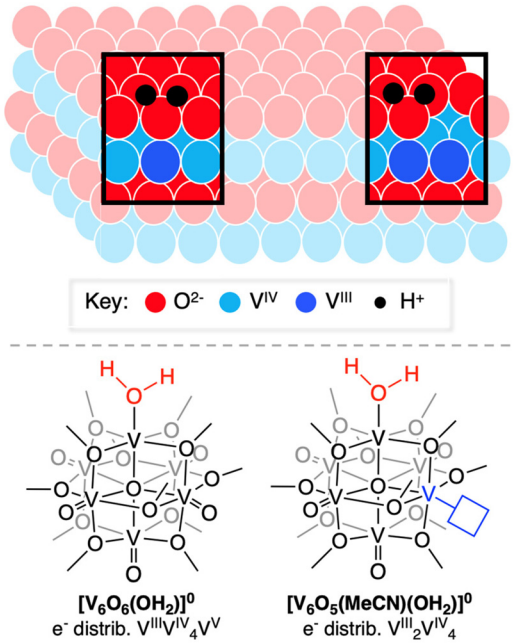

Fig. 1 PCET to the surface of pristine and O-deficient metal oxide surfaces (top). $2e^-/2H^+$ reduced POV–alkoxide clusters studied in this work, where V=O bond reduction occurs at the surface of a fully oxygenated vanadium oxide assembly, and one bearing a preformed O-atom vacancy to generate aquo-ligated cluster complexes.

reactivity of protons and H-atom equivalents to *terminal* oxide sites, resulting in the formation of an O-atom vacancy and water under appropriate reaction conditions.

One advantage to studying molecular systems as models for extended solids is the ability to manipulate the composition of the assemblies with atomic precision.[19] Indeed, our team has demonstrated formation of a POV–alkoxide cluster with *two* O-atom defect sites.[29] In that work, we established that surface O-atoms are removed sequentially from the cluster surface. Our ability to isolate and handle the "intermediate", $[V_6O_6(MeCN)(OCH_3)_{12}]^0$ (**$[V_6O_6(MeCN)]^0$**), allows for investigation of the impact embedded O-atom defects have on PCET in oxygen-deficient metal oxide assemblies.

Herein, we report the synthesis of two reduced forms of POV–alkoxide clusters with water ligated to surface of the assembly (Fig. 1). $[V_6O_6(OH_2)(OCH_3)_{12}]^0$ (**$[V_6O_6(OH_2)]^0$**) and $[V_6O_5((MeCN)(OH_2)(OCH_3)_{12}]^0$ (**$[V_6O_5(MeCN)(OH_2)]^0$**) are accessed *via* net multi H-atom transfer (HAT) to the fully oxygenated, neutral POV–alkoxide cluster, $[V_6O_7(OCH_3)_{12}]^0$ (**$[V_6O_7]^0$**), in tetrahydrofuran (THF). When HAT is performed in THF, the aquo ligand generated *via* PCET remains coordinated to the reduced V^{III} ion(s). This distinct attribute allows for experimental assessment of the $BDFE(O–H)_{avg}$ of the aquo O–H bonds. Analysis of the kinetics of net H-atom uptake reveals that while the mechanism of PCET proceeds *via* a concerted pathway in both examples, the presence of an O-atom defect accelerates the rate of net H-atom uptake by two orders of magnitude. Overall, this study reveals the impact O-atom defects have on PCET at metal oxides, providing insight into alterations of structural parameters that impact the reactivity of the surface with relevance to H-atom transfer chemistry.

Results & discussion

Initial studies probed addition of an excess of a potent H-atom transfer reagent to the neutral POV–alkoxide cluster, **$[V_6O_7]^0$**, to confirm that formation of the di-vacant POV–alkoxide cluster is possible *via* PCET. Upon addition of 2 equiv. of 5,10-dihydrophenazine (H_2Phen; $BDFE(N–H)_{avg}$ = 58.7 kcal mol^{-1})[30] in acetonitrile (MeCN), a colour change from green to red is observed (Scheme 1). Conversion to $[V_6O_5(MeCN)_2(OCH_3)_{12}]^0$ (**$[V_6O_5(MeCN)_2]^0$**) is completed within 3 min, as confirmed by ^{1}H NMR spectroscopy (Fig. S1;† see Experimental section for additional details). Formation of the oxidized H-atom transfer reagent, phenazine (Phen), is also observed in the ^{1}H NMR spectrum of the crude reaction mixture.

Formation of **$[V_6O_5(MeCN)_2]^0$** is similarly possible from the oxygen-deficient POV–alkoxide starting material, **$[V_6O_6(MeCN)]^0$**.

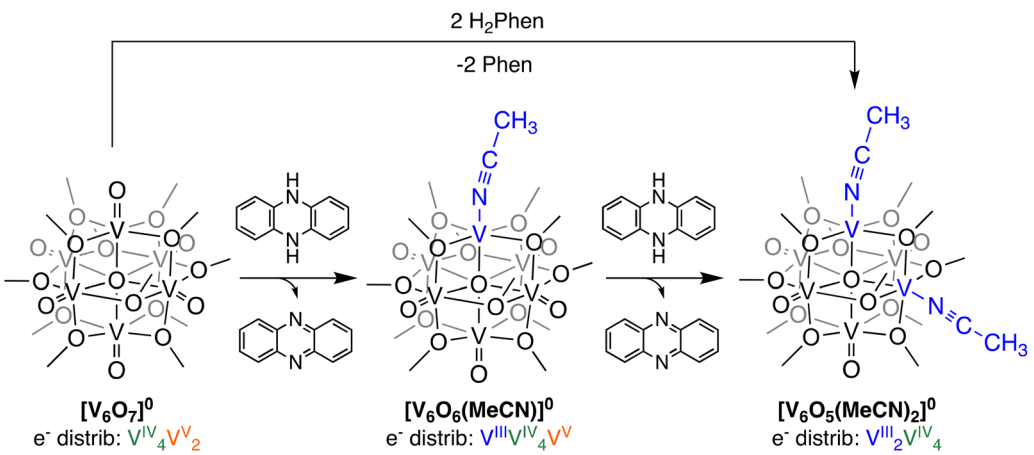

Scheme 1 Synthesis of O-atom vacancies in POV–alkoxide clusters *via* net H-atom uptake in MeCN; formation of **$[V_6O_6(MeCN)]^0$** and **$[V_6O_5(MeCN)_2]^0$**.

Addition of 1 equiv. of H_2Phen to $[V_6O_6(MeCN)]^0$ results in an instantaneous colour change from brown to red (Scheme 1). Analysis of the product distribution *via* ^{1}H NMR spectroscopy confirms formation of the di-vacant POV–alkoxide cluster, $[V_6O_5(MeCN)_2]^0$ and Phen (Fig. S2;† see Experimental section for additional details).

Thermodynamics of H-atom uptake in O-deficient POV–alkoxides

Our previous work summarizing the synthesis and characterization of O-atom deficient POV–alkoxide clusters includes electrochemical analysis of these assemblies. Cyclic voltammetry (CV) reveals a cathodic shift in open circuit potential of the assembly upon vacancy formation (Fig. 2). This observation is consistent with the formation of an electron-rich cluster core upon removal of an O-atom from the cluster surface. Accordingly, generation of a defect site results in a change in driving force for electron transfer to the assembly ($\Delta E_{1/2} \sim 0.3$ V).[29,31] We hypothesized that this change in redox potential would impact the thermodynamics of H-atom uptake and transfer at the surface of the cluster.

To understand the impact of an O-atom vacancy on the thermodynamics of H-atom uptake and transfer in POV–alkoxide clusters, we performed a series of equilibrium studies to determine BDFE(O–H)$_{avg}$ of surface aquo moieties. Previous work from our group has demonstrated that addition of H-atom transfer reagents to calix[4]arene-substituted POV–alkoxide clusters in tetrahydrofuran (THF) results in retention of the aquo ligand at the surface of the assembly.[15] We anticipate that similar stabilization of the surface aquo should occur in this system; therefore, all *in situ* equilibrium experiments reported here were conducted in THF-d_8.

Confirmation of H-atom installation and aquo-stabilization at the surface of the cluster was obtained through stoichiometric reactions with the parent POV–alkoxide cluster in THF. Exposure of $[V_6O_7]^0$ to 1 equiv. of hydrazobenzene (Hydz, BDFE(N–H)$_{avg}$ = 60.4 kcal mol^{-1}) in THF results in a rapid colour change from green to brown.[15] The ^{1}H NMR spectrum of the product in THF-d_8 reveals a reduction in symmetry of the vanadium-containing product ($O_h \rightarrow C_{4v}$) in analogy to previous results on V=O bond reduction in POV–alkoxides (Fig. S3†).[16,32] The three signals observed in the ^{1}H NMR spectrum of the product are slightly shifted (29.6, 16.2, −11.5 ppm) in comparison with the O-atom deficient analogue bearing a MeCN ligand (29.5, 15.7, −12.1 ppm; Fig. S4†). Analysis of the crude reaction mixture did not indicate formation of water, in contrast to results obtained previously in PCET reactions to POV–alkoxides in MeCN (Fig. S4†). This suggests that the aquo moiety formed upon addition of 2 H-atom equivalents to the V=O site remains coordinated to the surface of the cluster. Additional support for the formation of the aquo adduct, $[V_6O_6(OH_2)]^0$, was obtained from elemental analysis.

Recrystallization of the reduced POV–alkoxide was achieved by vapor diffusion of pentane directly into the reaction medium. The resultant crystals were suitable for analysis *via* single crystal X-ray diffraction (Fig. 3, and Table 1; see Table S1† for crystallographic parameters). Refinement of the data confirmed the identity of the reduced assembly to be the anticipated aquo-bound product, $[V_6O_6(OH_2)]^0$. The V1–O1 bond distance of 2.0671(19) Å is significantly elongated from that of the starting material, $[V_6O_7]^0$ (V=O$_t$ = 1.60 Å[33]), and consistent with V–O distances reported for vanadium(III) aquo complexes (1.967(3)–2.086(2) Å).[15,34,35] In particular, the V1–O1 distance resembles that reported by our research group for the calix[4]arene-substituted POV–alkoxide cluster featuring an

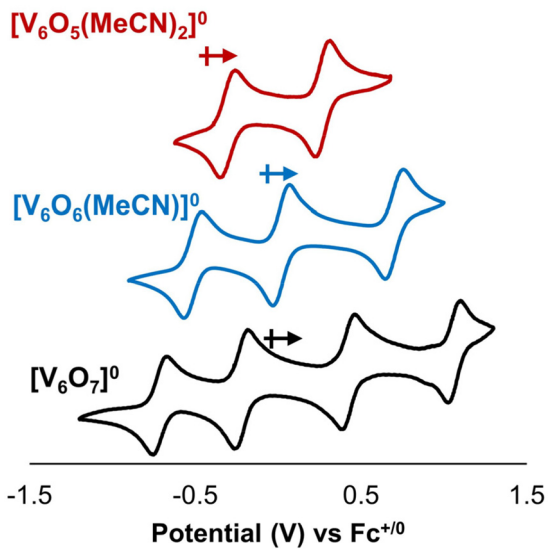

Fig. 2 Cyclic voltammograms of 1 mM $[V_6O_7]^0$ (black), $[V_6O_6(MeCN)]^0$ (blue), and $[V_6O_5(MeCN)_2]^0$ (red) in DCM with 100 mM [^{n}Bu$_4$N][PF$_6$] supporting electrolyte. Arrows indicate open circuit voltages of the individual cluster complexes in their neutral charge state. Figure reproduced with permission from B. E. Petel *et al.*, *Inorg. Chem.* 2019, **58**, 10462–10471. Copyright 2019 American Chemical Society.

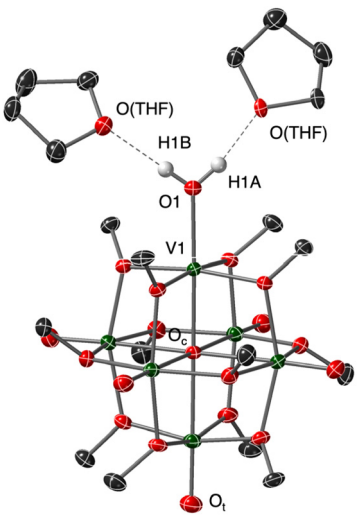

Fig. 3 Molecular structure of $[V_6O_6(OH_2)]^0$ shown with 50% probability ellipsoids. Selected hydrogen atoms have been omitted for clarity. Key: dark green ellipsoids: V; red ellipsoids: O; dark grey ellipsoids: C; white spheres: H.

Table 1 Selected bond distances from the X-ray crystal structure of $[V_6O_6(OH_2)]^0$ and $[V_6O_7]^0$[33]

Bond	$[V_6O_6(OH_2)]^0$	$[V_6O_7]^0$
V1–O1	2.0671(19) Å	—
V1–O_c	2.1158(16) Å	—
V=O_t (avg)	1.5998 Å	1.60 Å
V–O_c (avg)	2.3177 Å	2.28 Å
O1···O(THF)	2.640(14), 2.700(3) Å	—
O1–Hn···O(THF)	168(4), 175(5)°	—

aquo ligand, $[(calix)V_6O_5(OH_2)(MeCN)(OCH_3)_8]^0$ (V(III)-O(aquo) = 2.052(2) Å).[15] Further supporting our assignment of the aquo ligand are the identification of two THF molecules which serve as H-bond acceptors based on their orientation and proximity to the corresponding terminal O-atom (O1···O(THF) = 2.640(14), 2.700(3) Å; O1–Hn···O(THF) = 168(4), 175(5)°, n = 1A, 1B).

The formal transfer of two H-atom equivalents to the surface of $[V_6O_7]^0$ results in the reduction of the vanadium oxide core ($V^{IV}_4V^{V}_2 \rightarrow V^{III}V^{IV}_4V^{V}$). Fortunately, within the unit cell of $[V_6O_6(OH_2)]^0$, all V centres are located in general positions, providing an opportunity to interrogate the electronic structure of the cluster using bond valence sum calculations (Table S2†). Indeed, the oxidation state distribution of the reduced complex was found to be $V^{III}V^{IV}_4V^{V}$. We note that this formal assignment is relevant at low temperature (100 K) and in the solid state; in solution at elevated temperatures the V^V centre is expected to be delocalized about the fully oxygenated vanadium centres. This is evidenced by the observation of an intervalence charge transfer (IVCT) band diagnostic of $V^{IV} \rightarrow V^V$ electron transfer in the near infrared region of the electronic absorption spectrum of $[V_6O_6(OH_2)]^0$ (Fig. S5†).

With confirmation that water is stabilized at the surface of $[V_6O_6(OH_2)]^0$, we next sought to determine the strength of these surface O–H bonds. Determination of the experimental BDFE $(O–H)_{avg}$ of the surface H-atoms of $[V_6O_6(OH_2)]^0$ was achieved by exposure of the fully-oxygenated cluster to a reductant that does not react quantitatively with the complex in THF (Scheme 2). The generation of an equilibrium state allows us to invoke a modified version of the Nernst equation to find the adjusted BDFE(E–H) for the reductant, which under equilibrium conditions would be equivalent to the analogous parameter for the reduced cluster (Eqn (1)). Such analysis has been employed for studying surface O–H bonds on nanocrystalline ceria by Mayer and co-workers, as well as reduced POV–alkoxides by our group.[13,15,18] Equilibrium is reached after exposure of the cluster to various equivalents (0.5 to 2) of 1,4-dihydroxynaphthalene (H_2Naphth; $BDFE(O–H)_{avg}$: 62.6 kcal mol^{-1}) for 7 days in THF-d_8 (Fig. S6, and S7†).[30] Using the concentrations of the reductant and its oxidized partner, 1,4-naphthoquinone (Naphth), a value of n = 2 for the two H-atom equivalents transferred from the substrate, alongside Eqn (1), we determined the $BDFE(O–H)_{avg}$ of $[V_6O_6(OH_2)]^0$ to be 62.3 ± 0.1 kcal mol^{-1} (Table S3†).

$$BDFE_{adj} = BDFE_{H_2NQ} - \frac{1.364}{n} \times \log\frac{[H_2NQ]}{[NQ]} \quad (1)$$

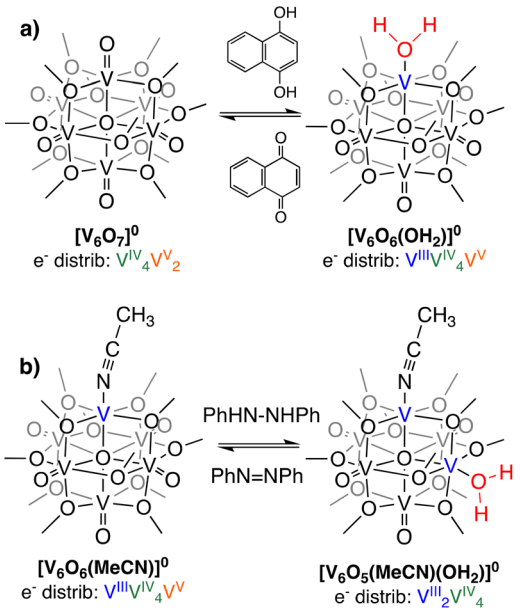

Scheme 2 Equilibrium reactions employed in the determination of $BDFE(O–H)_{avg}$ for (a) $[V_6O_6(OH_2)]^0$ and (b) $[V_6O_5(MeCN)(OH_2)]^0$.

Next, we set out to determine the $BDFE(O–H)_{avg}$ of the aquo ligand bound to a second O-atom deficient site at the surface of the assembly (Scheme 2). Despite the quantitative transfer of the H-atoms from Hydz ($BDFE(N–H)_{avg}$ = 60.4 kcal mol^{-1})[15,30] to $[V_6O_7]^0$, exposure of this reductant to $[V_6O_6(MeCN)]^0$ in THF-d_8 results in only partial conversion to the di-vacant cluster, $[V_6O_5(MeCN)(OH_2)(OCH_3)_{12}]^0$ ($[V_6O_5(MeCN)(OH_2)]^0$) (Fig. S9†). After 15 days, the concentrations of Hydz and its oxidized counterpart, azobenzene (Azo) remain static, indicating the system has reached equilibrium (Fig. S10†). Measuring the respective concentrations of reduced and oxidized substrate at equilibrium, the $BDFE(O–H)_{avg}$ of the aquo ligand bound to $[V_6O_5(MeCN)(OH_2)]^0$ was determined to be 60.7 ± 0.1 kcal mol^{-1} (Table S4†).

The observed decrease in $BDFE(O–H)_{avg}$ from $[V_6O_6(OH_2)]^0$ to $[V_6O_5(MeCN)(OH_2)]^0$ highlights the impact of the oxidation state distribution of distal vanadium ions on the thermodynamics of PCET at the cluster surface. This is consistent with results published by Agapie and coworkers for a "Fe_3Mn" cluster, in which electron-rich variants of these multimetallic compounds exhibit weak Mn(O–H) bond strengths in comparison to their oxidized derivatives.[36] Our group has corroborated this trend, observing that the strength of surface O–H bonds located at both terminal and bridging positions of Lindqvist-type POV–alkoxide clusters is dependent on the degree of reduction of the constituent metal ions; in all examples, reduced forms of the vanadium oxide assemblies possess the lowest BDFE(O–H) values.[14,16,20] The influence of oxidation state of metal centres in multimetallic configurations on the thermodynamics of PCET is also observed in nanocrystalline metal oxides, as shown in recent reporting from Mayer and coworkers.[13]

Kinetic analysis of PCET in oxygen-deficient POV–alkoxides

With an understanding of the impact of an O-atom defect on the thermodynamics of H-atom uptake in POV–alkoxide clusters, our attention turned to observed discrepancies in the rates of PCET at the surface of $[V_6O_7]^0$ and $[V_6O_6(MeCN)]^0$. According to Marcus Theory, relative rates of net H-atom transfer between two substrates are directly proportional to the ΔBDFE(E–H) between H-atom donor and acceptor; ΔBDFE(E–H), or driving force, influences equilibrium constants (K_{eq}) in H-atom transfer reactions, thus impacting the observed rate of reaction for a system.[37] Based on these considerations alone, we hypothesized that the rate of H-atom uptake and O-atom vacancy formation in $[V_6O_6(MeCN)]^0$ would be slower than that of its fully oxygenated congener, $[V_6O_7]^0$, given the resultant O–H bonds are weaker in the further reduced, O-atom deficient assembly.

To evaluate our hypothesis, a series of kinetic analyses were performed in which electronic absorption spectroscopy was used to monitor cluster reduction. This approach leverages the differentiated spectra of $[V_6O_6(MeCN)]^0$ and $[V_6O_5(MeCN)(OH_2)]^0$. The more oxidized cluster, $[V_6O_6(MeCN)]^0$ (oxidation state distribution: $V^{III}V_4^{IV}V^V$) features an intervalence charge transfer (IVCT) band, corresponding to electron transfer between the V^{IV} and V^V ions in the core (λ = 900 nm (ε = 413 M^{-1} cm^{-1}.[29] The reduced species lacks V^V ions (oxidation state distribution: $V_2^{III}V_4^{IV}$), dramatically reducing its absorptivity at 900 nm (ε < 100 M^{-1} cm^{-1}, Fig. S13, and S14†).[29] As such, the change in absorbance at 900 nm was monitored upon addition of an excess of H_2Phen to $[V_6O_6(MeCN)]^0$ (Fig. S15–20,† see Experimental section for details). Fitting of the generated traces produces a linear plot when correlating the observed pseudo first-order rate constant, k_{obs} to the reductant concentration (Fig. 4). This observation indicates that the rate-determining step is first order in both reductant and cluster (Eqn (2)). Notably, kinetic analyses on net H-atom uptake at the surface of the fully-oxygenated cluster, $[V_6O_7]^0$, similarly reveal a second-order rate-limiting process.[16] The analogous rate expressions provide an initial indication that both clusters undergo net H-atom uptake *via* similar mechanisms.

$$\frac{d[V_6O_5(MeCN)(OH_2)]}{dt} = k[H_2Phen]^1[V_6O_6(MeCN)]^1 \qquad (2)$$

In our previous study, the formation of an O-atom defect at $[V_6O_7]^0$ by PCET was determined to proceed *via* two concerted proton–electron transfer (CPET) reactions.[16] We thus hypothesized that a CPET mechanism is similarly operative for the reduction of $[V_6O_6(MeCN)]^0$. Kinetic isotope effect (KIE) experiments, employing the deuterium-labelled reductant, D_2Phen, reveal a substantial KIE (4.4). This finding disqualifies a potential electron transfer–proton transfer (ET–PT) mechanism (Fig. 4 and Table 2). This is supported by electrochemistry experiments, which found that the oxidation potential of H_2Phen ($E_{1/2}$ = −0.387 V *vs.* $Fc^{+/0}$, Fig. S11†) is not sufficiently reducing to transfer an electron to $[V_6O_6(MeCN)]^0$ ($E_{1/2}$ = −0.646 V *vs.* $Fc^{+/0}$, Fig. S12.†)

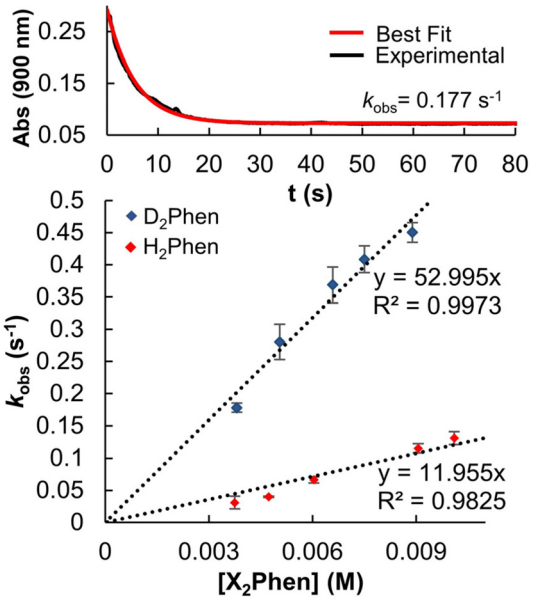

Fig. 4 Determination of the observed pseudo first-order rate constant, k_{obs}, for the reduction of $[V_6O_6(MeCN)]^0$ (0.75 mM) by H_2Phen (3.81 mM) in MeCN at −15 °C by monitoring absorbance at 900 nm over the reaction coordinate (top). Plot of k_{obs} as a function of [X_2Phen], where X = H, D. Concentration of $[V_6O_6(MeCN)]^0$ was held constant at 0.75 mM, and reductant concentration was varied between 3.8 and 11.5 mM. The slope of the resultant lines * $\frac{1}{4}$ vanadyls possible for accepting the H-atom * $\frac{1}{2}$ for the two chemically equivalent H-atoms transferred provides the experimentally derived second-order rate constants, k_{PCET}. Comparison of k_{PCET} for H_2Phen and D_2Phen yields a KIE of 4.4.

Table 2 Thermodynamic and kinetic parameters of defect formation *via* PCET in POV–alkoxide clusters

	$[V_6O_6(OH_2)]^0$ [16]	$[V_6O_5(MeCN)(OH_2)]^0$
$BDFE(O–H)_{avg}$	62.3 ± 0.1 kcal mol^{-1}	60.7 ± 0.1 kcal mol^{-1}
k_{PCET}@298 K	0.14 ± 0.05 M^{-1} s^{-1}	19.6 ± 3.2 M^{-1} s^{-1}
KIE	2.1	4.4
$\Delta H^{\ddagger}$ (kcal mol^{-1})	7.8 ± 0.8	4.3 ± 1.2
$\Delta S^{\ddagger}$ (cal mol^{-1} K^{-1})	−31.0 ± 3.3	−33.9 ± 4.8
$\Delta G^{\ddagger}$ (kcal mol^{-1})	18.7 ± 1.7	14.4 ± 2.6

The proton transfer–electron transfer (PT–ET) pathway is similarly eliminated due to the weak acidity of the organic substrate, as the deprotonation of a neutral amine is unlikely to occur in the absence of a strong base (*e.g.* Na metal).[38] To determine the relative basicities of each reactive species, we employ the following equation popularized by Bordwell,[39–41]

$$BDFE(E–H) = 1.37(pK_a) + 23.06(E^{\circ}) + C_G \qquad (3)$$

where BDFE(E–H) is the homolytic BDFE of the bond in question, pK_a is the acidity of the E–H proton, E^0 is the redox potential of the compound, and C_G is a constant related to the reduction of a proton to a H-atom radical in a given solvent. This allows us to use the thermochemical steps outlined in a

square scheme for both PCET reactions (*i.e.* H-atom transfer from H_2Phen and H-atom installation onto $[V_6O_6(MeCN)]^0$, Scheme 3).

Using the established BDFE(N–H)$_{avg}$ of H_2Phen in THF (59.2 kcal mol^{-1}), the average reduction potential for 2e$^-$ reduction of Phen (−2.15 V *vs.* $Fc^{+/0}$), and C_G for THF (59.9 kcal mol^{-1}), we can apply this function to find the average pK_a for the protons bound to reduced $[Phen]^{2-}$ to be 35.6. Similarly, using the BDFE(O–H)$_{avg}$ of $[V_6O_5(MeCN)(OH_2)]^0$ from equilibrium experiments (60.7 ± 0.1 kcal mol^{-1}), oxidation potentials of this compound (−0.325 V, 0.222 V *vs.* $Fc^{+/0}$, Fig. S12†), and C_G, we find the average pK_a for the protonated intermediate of $[V_6O_6(MeCN)]^0$ ("$[V_6O_5(MeCN)(OH_2)]^{2+}$") to be 1.45. This indicates that the complex is a significantly weaker base than $[Phen]^{2-}$ and thus will not deprotonate H_2Phen.

Additional evidence in support of a CPET mechanism is provided in the assessment of activation parameters obtained from variable temperature kinetics experiments. Construction of an Eyring plot allows for the determination of activation parameters for the rate-determining step of the PCET reaction (Fig. 5, and Table 2). We find that the activation entropy, $\Delta S^{\ddagger}$, of net H-atom uptake reactions at the surface of $[V_6O_7]^0$ and $[V_6O_6(MeCN)]^0$ are similarly large in magnitude and negative in sign, while the enthalpic contributions to the overall activation barrier, $\Delta H^{\ddagger}$, are comparatively small. These results suggest that the rate-determining step involves an inner-sphere process with a highly ordered transition state. Similar observations have been made in previous examples of net H-atom transfer reactivity invoked to occur through a CPET-type mechanism.[14–16,18,20,42,43] Collectively, these findings support the hypothesis that generation of the aquo moiety in $[V_6O_5(MeCN)(OH_2)]^0$ occurs *via* a rate-determining CPET process.

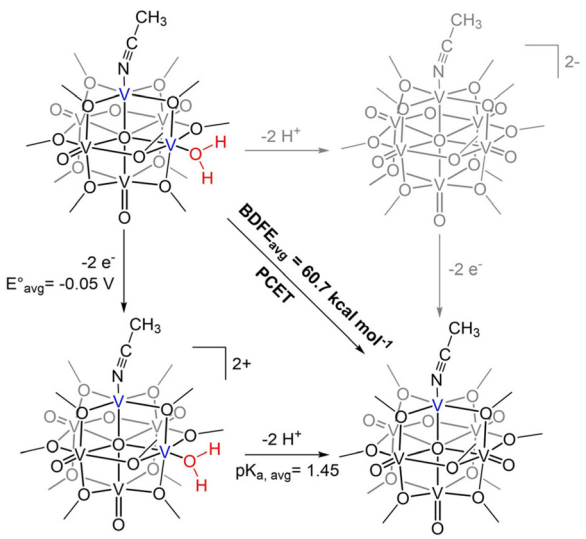

Scheme 3 Square scheme of 2e$^-$/2H$^+$ reduction of $[V_6O_6(OH_2)]^0$ to $[V_6O_5(MeCN)(OH_2)]^0$.

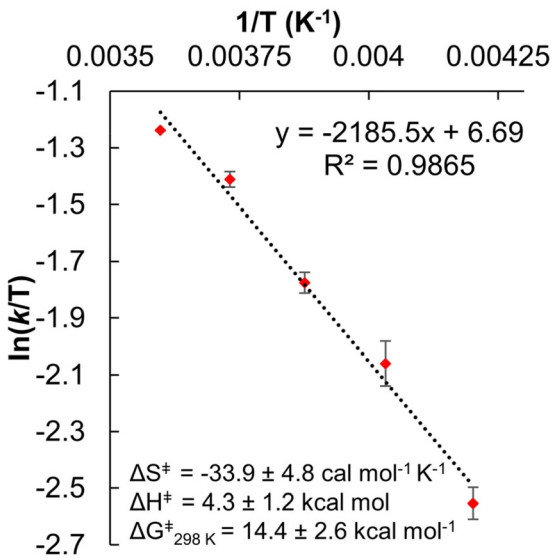

Fig. 5 Eyring plot for the reaction of $[V_6O_6(MeCN)]^0$ (0.75 mM) with H_2Phen (7.3 mM) in MeCN between −35 and 15 °C. *Y*-Axis values were determined by dividing k_{obs} by the concentration of H_2Phen, providing the rate constant, k_{PCET}. Activation parameters are labelled on the plot.

With mechanistic insights in hand, we sought to evaluate how the O-atom defect site alters the rate of PCET to the cluster surface. The rate constant for the reduction of $[V_6O_6(MeCN)]^0$ from H_2Phen can be extrapolated from the Eyring plot at a given temperature, which was determined to be 19.6 ± 3.2 M^{-1} s^{-1} at 25 °C (Fig. 5 and Table 2). This corresponds with a 100-fold increase in reaction rate over that reported for $[V_6O_7]^0$ at the same temperature (0.14 ± 0.05 M^{-1} s^{-1}).[16]

The acceleration in rate of net H-atom uptake at $[V_6O_6(MeCN)]^0$ is striking considering the reduction of thermodynamic driving force for PCET (smaller ΔBDFE(O–H), *vide supra*). To justify this observation, we considered the activation parameters derived from Eyring analysis (Table 2). As described above, the entropy of activation ($\Delta S^{\ddagger}$) in both reactions are large, negative values. Our lab and others have shown that $\Delta S^{\ddagger}$ values of this magnitude are consistent with a well-ordered intermediate, suggesting the existence of a hydrogen bonded complex between the H-atom donor and acceptor in the transition state.[14–16,18,20,42,43] The observation of comparable values of $\Delta S^{\ddagger}$ is unsurprising, as both transition states involve the preorganization of reductant and cluster in close proximity. However, in comparing the enthalpies of activation ($\Delta H^{\ddagger}$) of H-atom transfer to fully oxygenated and O-atom deficient POV–alkoxide clusters, we note a significant discrepancy; while both values are consistent with previously reported CPET reactions to metal oxide surfaces, the small $\Delta H^{\ddagger}$ associated with formation of $[V_6O_5(MeCN)(OH_2)]^0$ indicates that less energy is required for bond weakening processes relevant to the formation of the transition state.[14–16,18,20,42,43]

We attribute the reduction in $\Delta H^{\ddagger}$ to the increased electron density in the core of the oxygen-deficient POV–alkoxide cluster, $[V_6O_6(MeCN)]^0$. Injection of reducing equivalents into

POV–alkoxide clusters has been previously shown to increase the basicity of terminal V=O units;[44] similarly, the electron donor character of the O-deficient V^{III} centre should lead to greater nucleophilicity of the remaining oxygenated sites. Indeed, determination of the average pK_a's of the corresponding acids (represented as "$[V\text{–}OH_2]^{2+}$" in the thermochemical square scheme (Scheme 3)) of $\mathbf{[V_6O_7]^0}$ (pK_a = −1.98) and $\mathbf{[V_6O_6(MeCN)]^0}$ (pK_a = 1.45) found that the defect-containing species was more basic than its fully oxygenated congener (Table S6†). The rate of CPET has been shown in several reports to be tuneable with the pK_a of the proton or H-atom acceptor, with more basic acceptors producing accelerated reaction rates.[45–48] This is due to the influence of pK_a on ΔBDFE(E–H), as well as transition state thermodynamics. In a variety of cases, donor/acceptor pK_a has been shown to correlate more strongly to PCET rate constants than ΔBDFE(E–H), describing an imbalanced transition state with more proton transfer character and an asynchronous CPET mechanism.[47,49–55] An example from Hammes–Schiffer and coworkers describes the influence of proton transfer free energy (ΔG°_{PT}), related to pK_a, on CPET in fluorenyl-benzoates, revealing that this thermodynamic parameter contributes to the proton donor–acceptor distance in the transition state.[56] By increasing the relative basicity of the acceptor, this distance is minimized, decreasing the energetic requirement to facilitate proton tunnelling. In the present study, the increased surface basicity of the O-deficient POV–alkoxide is then expected to produce an H-bond with H_2Phen with lower energetic cost than its fully-oxygenated partner, supported by a lower $\Delta H^\ddagger$. Therefore, despite the greater driving force exhibited for PCET to $\mathbf{[V_6O_7]^0}$, the more basic surface of the O-atom deficient POV–alkoxide results in an accelerated rate of PCET to $\mathbf{[V_6O_6(MeCN)]^0}$.

Conclusions

Here, we present an alternative approach for tuning the thermodynamics and kinetics of net H-atom uptake and transfer at metal oxide surfaces by introducing a structurally distinct, redox-inactive V^{III} ion into the cluster structure *via* defect engineering. The reduced site in $\mathbf{[V_6O_6(MeCN)]^0}$ functions as an anionic dopant, injecting electron density into the cluster core.[29,31] Comparative studies on the strength of surface O–H bonds formed upon reduction of a V^V-oxo to a V^{III}-aquo in this O-deficient assembly with its more oxidized congener, $\mathbf{[V_6O_7]^0}$, find that this additional electron density serves to weaken these bonds by ∼2 kcal mol^{-1}. Kinetic analyses of these systems reveal, however, that despite this decrease in driving force, the O-deficient species undergoes PCET at rates two orders of magnitude higher than the respective oxygenated complex. This system breaks the expected driving force/rate scaling relationship predicted by Marcus Theory as a consequence of the increased electron density in this cluster, which imparts higher relative basicity to the remaining V=O moieties of $\mathbf{[V_6O_6(MeCN)]^0}$ and allows for facile access to the transition state. Taken together, this work reveals how doping can serve to tune PCET processes at molecular metal oxides, furthering our understanding of these systems and providing new perspectives on analogous processes in reducible metal oxide materials.

Experimental

General considerations

All manipulations were carried out in the absence of water and oxygen using standard Schlenk techniques or in a UniLab MBraun inert atmosphere drybox under a dinitrogen atmosphere. All glassware was oven-dried for a minimum of 4 h and cooled in an evacuated antechamber prior to use in the drybox. Solvents were dried and deoxygenated on a glass contour system (Pure Process Technology, LLC) and stored over 3 Å molecular sieves purchased from Fisher Scientific and activated prior to use. 5,10-Phenazine (Phen), hydrazobenzene (Hydz), 1–4-naphthoquinone (Naphth), and 1.6 M ^{n}butyllithium in hexanes were purchased from Sigma-Aldrich and used as received. D_2O was purchased from Cambridge Isotope Laboratories and used as received. $[V_6O_7(OCH_3)_{12}]^0$,[33] $[V_6O_6(OCH_3)_{12}]^0$,[29] 1,4-dihydroxynaphthalene (H_2Naphth),[57] 5,10-dihydrophenazine (H_2Phen),[58] and its deuterated analogue (D_2Phen)[16] were generated according to literature precedent.

^{1}H NMR spectra were recorded at 500 MHz on a Bruker DPX500 spectrometer locked on the signal of deuterated solvents. All chemical shifts were reported relative to the peak of the residual H signal in deuterated solvents. CD_3CN and THF-d_8 were purchased from Cambridge Isotope Laboratories, degassed by three freeze–pump–thaw cycles, or received in a glass ampule, and stored over fully activated 3 Å molecular sieves. UV-Vis-NIR spectroscopy was collected using an Agilent Cary 6000i spectrophotometer at 21 °C and −35 °C. Samples were prepared in the drybox in MeCN or THF and added to airfree cuvettes and sealed prior to removing from the drybox. All molar absorptivity values were determined by averaging spectra collected in triplicate at different concentrations. Kinetics experiments were carried out on an Agilent Cary 60 UV-Vis-NIR spectrophotometer held at desired temperatures using an Unisoku CoolSpek UV cryostat.

Cyclic voltammetry (CV) was performed using a BioLogic SP 150 potentiostat/galvanostat and the EC-Lab software suite. Glassy carbon discs (3 mm, CH Instruments, USA) were used as working electrodes. Working electrodes were polished using a micro cloth pad and 0.05 μM alumina powder. Potentials recorded during CV were measured relative to a nonaqueous Ag/Ag^+ reference electrode with 1 mM $AgNO_3$ and 100 mM $[^nBu_4N][PF_6]$ in MeCN (BASi) and ultimately referenced against the $Fc^{+/0}$ couple using an internal reference. A platinum wire served as the counter electrode. All experiments were carried out at room temperature inside a nitrogen-filled glove box (MBraun, USA). All CV measurements were iR compensated at 85% with impedance taken at 100 kHz using the ZIR tool

included with the EC-Lab software. CV experiments were conducted at 100 mV s^{-1} on solutions of either 2 or 1 mM analyte and 200 mM [^{n}Bu$_4$N][PF$_6$] supporting electrolyte in THF.

A single crystal of $[V_6O_6(OH_2)]^0$ was placed onto a thin glass optical fibre and mounted on a Rigaku XtaLAB Synergy-S Dualflex diffractometer equipped with a HyPix-6000HE HPC area detector for data collection at 100.00(10) K. A preliminary set of cell constants and an orientation matrix were calculated from a small sampling of reflections.[59] A short pre-experiment was run, from which an optimal data collection strategy was determined. The full data collection was carried out using a PhotonJet (Cu) X-ray source with frame times of 0.55 and 2.20 seconds and a detector distance of 34 mm. Series of frames were collected in 0.50° steps in ω at different 2θ, κ, and ϕ settings. After the intensity data were corrected for absorption, the final cell constants were calculated from the *xyz* centroids of 26 024 strong reflections from the actual data collection after integration.[39] See Table S1 (ESI†) for additional crystal and refinement information. The structure was solved using SHELXT[60] and refined using SHELXL.[61] The space group $P\bar{1}$ was determined based on intensity statistics. All non-hydrogen atoms were refined with anisotropic displacement parameters. All other hydrogen atoms were placed in ideal positions and refined as riding atoms with relative isotropic displacement parameters. The final full matrix least squares refinement converged to R_1 = 0.0360 (F^2, $I > 2\sigma(I)$) and wR_2 = 0.1030 (F^2, all data). Elemental analysis was performed on a PerkinElmer 2400 Series II Analyzer, at the CENTC Elemental Analysis Facility, University of Rochester.

Synthesis of $[V_6O_5(MeCN)_2]^0$

(**Method A**) A 20 mL scintillation vial was charged with $[V_6O_7]^0$ (0.034 g, 0.042 mmol), H_2Phen (0.002 g, 0.085 mmol, 2 equiv.), and 6 mL of MeCN. The reaction was stirred for 30 min to ensure completion, after which the solvent was removed under reduced pressure to yield a brown solid. The solid was stirred in pentane (10 mL) for 30 min. The solid was then filtered and continuously washed with pentane until the filtrate ran clear (~15 mL). The solid was then extracted with MeCN, and any volatiles were removed under vacuum to yield $[V_6O_5(MeCN)_2]^0$ (0.027 g, 0.033 mmol, 79%). Characterization of the product, $[V_6O_5(MeCN)_2]^0$, matched that previously reported by our research group.[29]

(Method B) A 20 mL scintillation vial was charged with $[V_6O_6(MeCN)]^0$ (0.018 g, 0.022 mmol), H_2Phen (0.005 g, 0.024 mmol, 1.1 eq.) and 6 mL of MeCN. The reaction was stirred 30 min to ensure completion and the solvent was removed under reduced pressure to yield a red solid. The solid was stirred in pentane (10 mL) for 30 min to remove phenazine byproduct. The solid was then extracted in MeCN and volatiles were removed under vacuum to yield $[V_6O_5(MeCN)_2]^0$ (0.031 g, 0.016 mmol, 73%) Characterization of the product, $[V_6O_5(MeCN)_2]^0$, matched that previously reported by our research group.[29]

Synthesis of $[V_6O_6(OH_2)]^0$

A 20 mL scintillation vial was charged with $[V_6O_7]^0$ (0.010 g, 0.013 mmol), Hydz (0.003 g, 0.014 mmol, 1 equiv.), and 6 mL of THF. The reaction was stirred for 2 h, after which the solvent was removed under reduced pressure to yield a brown solid. The solid was stirred in pentane (10 mL) for 30 min, and subsequently filtered and continuously washed with pentane until the filtrate ran clear. The solid was then extracted with THF, and any volatiles were removed under vacuum to yield the product, $[V_6O_6(OH_2)]^0$, in good yield (0.007 g, 0.009 mmol, 69%). Crystals suitable for X-ray analysis were grown from the vapour diffusion of pentane into a crude reaction mixture in THF. ^{1}H NMR (500 MHz, THF-d_8): δ = 29.6, 16.2, −11.5 ppm. UV–vis (THF): 385 nm (ε = 2748 M^{-1} cm^{-1}), 544 nm (ε = 306 M^{-1} cm^{-1}), 1029 nm (ε = 533 M^{-1} cm^{-1}). Elemental analysis for $V_6O_{18}C_{12}H_{36}\cdot 1OH_2\cdot 0.15OC_4H_8$ (MW: 802.88 g mol^{-1}) Calc'd (%): C, 18.85; H, 4.92. Found (%): C, 18.920; H, 4.739.

Synthesis of $[V_6O_5(MeCN)(OH_2)]^0$

A 20 mL scintillation vial was charged with $[V_6O_6(MeCN)]^0$ (0.024 g, 0.029 mmol), H_2Phen (0.006 g, 0.030 mmol, equiv), and 6 mL of THF. The reaction was stirred for 2 h to ensure completion, after which the solvent was removed under reduced pressure to yield a red solid. The solid was stirred in pentane (10 mL) for 30 min. The solid was then filtered and continuously washed with pentane until the filtrate ran clear. The solid was then extracted with THF, and any volatiles were removed under vacuum to yield $[V_6O_5(MeCN)(OH_2)]^0$ (0.021 g, 0.025 mmol, 87%). ^{1}H NMR (500 MHz, THF-d_8): δ 27.43, −2.35, −3.37, −7.17, −21.52 ppm. UV–vis (THF): 440 nm (ε = 625 M^{-1} cm^{-1}), 535 nm (ε = 361 M^{-1} cm^{-1}), 950 nm (ε = 98 M^{-1} cm^{-1}). Elemental analysis for $V_6O_{17}C_{12}H_{36}\cdot 1OH_2\cdot 1OC_4H_8\cdot 0.1C_2H_3N$ (MW: 852.28 g mol^{-1}) Calc'd (%): C, 22.83; H, 5.48, N, 0.16. Found (%): C, 22.732; H, 5.086; N, 0.250.

Procedure for thermochemical analysis of the BDFE(O–H) of $[V_6O_6(OH_2)]^0$ and $[V_6O_5(MeCN)(OH_2)]^0$

Determination of the BDFE(O–H)$_{avg}$ of $[V_6O_6(OH_2)]^0$ was performed using reactions between $[V_6O_7]^0$ and 0.5–2 equivalents of 1,4-dihydroxynaphthalene (H_2NQ). 300 μL of cluster stock solution (14.2 mM) and the appropriate volume (116–348 μL) of reductant solution (24.4 mM) in THF-d_8 were combined in a J. Young tube and sealed prior to removal from the glovebox for analysis. Reactions were allowed to equilibrate over 7 days at room temperature, tracking progress by ^{1}H NMR (Fig. S6†). Upon equilibration, the relative concentrations of naphthoquinone (NQ) to H_2NQ were determined by using the integrations of resonances corresponding with each compound and normalizing for the number of protons each signal represents (Table S3†). Upon determination of [H_2NQ]/[NQ], the adjusted BDFE of the reductant was determined for each reaction using the following equation:

$$\mathrm{BDFE_{adj}} = \mathrm{BDFE_{H_2NQ}} - \frac{1.364}{n} \times \log \frac{[\mathrm{H_2NQ}]}{[\mathrm{NQ}]}$$

where $BDFE_{H_2NQ}$ is the average BDFE(O–H) of the O–H bonds in H_2NQ (62.6 kcal mol^{-1}),[30] n is the number of H-atom equivalents transferred (n = 2), and $BDFE_{adj}$ is the adjusted BDFE of the reductant O–H bonds under the reaction conditions.[13] Averaging the observed $BDFE_{adj}$ values provides the equilibrium $BDFE_{adj}$ for the reductant, which is equivalent to that of the O–H bond of $\mathbf{[V_6O_6(OH_2)]^0}$. This was found to be 62.3 ± 0.1 kcal mol^{-1} (Table S3†).

Determination of the $BDFE(O–H)_{avg}$ of $\mathbf{[V_6O_5(MeCN)(OH_2)]^0}$ was performed using reactions between $\mathbf{[V_6O_6(MeCN)]^0}$ and 1 equivalent of Hydz in triplicate. 207 μL of cluster stock solution (7.73 mM) and 115 μL of reductant (13.9 mM) in THF-d_8 and 78 μL of THF-d_8 were combined in a J. Young tube and sealed prior to removal from the glovebox for analysis. Reactions were allowed to equilibrate over 15 days at room temperature, tracking progress by ^{1}H NMR (Fig. S9†). Upon equilibration, the relative concentrations of azobenzene (Azo) to Hydz were determined by using the integrations of resonances corresponding with each compound and normalizing for the number of protons each signal represents (Table S4†). Upon determination of [Hydz]/[Azo], the adjusted BDFE of the reductant was determined for each reaction as above, where $BDFE_{Hydz}$ = 60.4 kcal mol^{-1} [30] and n = 2. Averaging the observed $BDFE_{adj}$ values finds the $BDFE(O–H)_{avg}$ of $\mathbf{[V_6O_5(OH_2)]^0}$ to be 60.7 ± 0.1 kcal mol^{-1} (Table S4†).

Procedure for kinetic analyses of PCET at $\mathbf{[V_6O_5(MeCN)(OH_2)]^0}$

Pseudo-first order reaction conditions were used to establish the rate constant of the PCET reaction between $\mathbf{[V_6O_6(MeCN)]^0}$ and H_2Phen at −15 °C in MeCN. Using a UV-Vis-NIR spectrometer with an N_2-cooled cryostat set to −15 °C, reactions between $\mathbf{[V_6O_6(MeCN)]^0}$ and excess H_2Phen (5.0–13.5 equivalents) were tracked by monitoring the absorbance at 900 nm. Final reductant concentrations were varied from 3.75 to 10.16 mM, with a constant concentration of cluster of 0.75 mM. A 3 mL sample of $\mathbf{[V_6O_6(MeCN)]^0}$ was loaded in a quartz cuvette, sealed with a septum, and was allowed to equilibrate to −15 °C, at which time the spectrometer began collecting absorbance data. After ∼20 seconds, 0.3 mL of reductant stock solution (38.1 mM) was forcefully injected to ensure homogeneity in the sample. As the PCET reaction progressed, the absorbance decayed until the reaction reached completion, levelling to the absorbance for $\mathbf{[V_6O_5(MeCN)_2]^0}$. The plots of absorbance over time were fit to the following equation by least squares fitting (Fig. S15–19†):

$$A_t = A_f + (A_i - A_f)e^{-k_{obs}t}$$

where A_t is the calculated absorbance at time, t, in seconds, A_f is the absorbance value at the end of the experiment, A_i is the initial absorbance after injection of cluster to the cuvette, and k_{obs} is the pseudo-first order rate constant. The excellent fit found for reaction curves indicated that the order of reductant in the rate expression was 1. Each experiment was repeated in triplicate. Plotting k_{obs} as a function of reductant concentration generated a linear plot, meaning that the reaction rate expression is second order overall, such that:

$$\frac{d[V_6O_5(MeCN)_2]}{dt} = k[H_2Phen]^1[V_6O_6(MeCN)]^1$$

The slope of the line, when held to a y-intercept of 0, of 52.99 (R^2 = 0.9973), provides the experimentally determined rate constant, k_{PCET} at −15 °C of 6.6 ± 0.3 M^{-1} s^{-1}, which accounts for the two H-atoms from the H_2Phen and four possible V=O reactive sites. To determine the kinetic isotope effect (KIE), analogous reactions were carried out at −15 °C using 3 mL samples of D_2Phen solution between 3.75 and 10.1 mM, and 0.44 mL of cluster stock solution (5.14 mM) for a 0.75 mM final concentration (Fig. S20–24†). Experiments were repeated in triplicate. Similar treatment of the data produced a k_{PCET} for the formation of deuterium-labelled species of 1.49 ± 0.05 M^{-1} s^{-1}.

Procedure for determination of activation parameters

Eyring analysis was performed by collecting absorbance *vs.* time data at temperatures between −35 and 5 °C. Reactions were assembled in an analogous fashion to the above kinetics experiments, with constant reductant and cluster concentrations of 0.75 mM and 7.26 mM, respectively. Experiments were repeated in triplicate. Conversion of k_{obs} to k_{PCET} was done by dividing k_{obs} by the reductant concentration and number of sites available for PCET (4 equatorial vanadyls) and number of H-atoms (2). Plotting $\ln(k_{PCET}/T)$ as a function of $1/T$ (temperature converted to K), the linear plot was used to solve for activation parameters using the below equations where R is the gas constant in units of cal/(mol K), k_{Boltz} is Boltzmann's constant, and h_{Planck} is Planck's constant. The activation parameters for the reduction of $\mathbf{[V_6O_6(MeCN)]^0}$ are listed in Fig. 5 and S25–28.†

$$\ln\left(\frac{k_{PCET}}{T}\right) = -2273.5 \times \frac{1}{T} + 7.0695$$

$$\Delta H^{\ddagger} = -2273.5 \times R$$

$$\Delta S^{\ddagger} = R \times \left[7.0695 - \ln\left(\frac{k_{Boltz}}{h_{Planck}}\right)\right]$$

$$\Delta G^{\ddagger} = \Delta H^{\ddagger} - T\Delta S^{\ddagger}.$$

Author contributions

S.E.C, E.S., and E.M.M conceived all experiments. E.S. performed the synthesis and crystallization of $\mathbf{[V_6O_6(OH_2)]^0}$, as well as all cyclic voltammetry and scanning kinetics experiments. All remaining syntheses and experimental data were performed and collected by S.E.C, except those involving X-Ray crystallography. W.W.B. collected single crystal X-Ray diffraction data and solved the crystal structure. All authors contributed to the writing of the manuscript.

Conflicts of interest

There are no conflicts to declare.

Acknowledgements

This research was funded by the National Science Foundation (CHE-2154727). E. M. M. is also a recipient of a Camille Dreyfus Teacher-Scholar Award from The Camille & Henry Dreyfus Foundation which has provided additional resources to support this work. E. S. is a recipient of the Messersmith Fellowship from the University of Rochester which has provided support for this study.

References

1 H. Ritchie and M. Roser, Our World in Data: Renewable Energy **https://ourworldindata.org/renewable-energy**.
2 R. F. Service, Solar plus batteries is now cheaper than fossil power, *Science*, 2019, **365**, 108.
3 U. S. E. I. Adminitration, *International Energy Outlook* 2020 **https://www.eia.gov/outlooks/ieo/**.
4 P. De Luna, C. Hahn, D. Higgins, S. A. Jaffer, T. F. Jaramillo and E. H. Sargent, What would it take for renewably powered electrosynthesis to displace petrochemical processes?, *Science*, 2019, **364**, eaav3506.
5 J. L. Dempsey, J. R. Winkler and H. B. Gray, Proton-Coupled Electron Flow in Protein Redox Machines, *Chem. Rev.*, 2010, **110**, 7024.
6 M. H. V. Huynh and T. J. Meyer, Proton-Coupled Electron Transfer, *Chem. Rev.*, 2007, **107**, 5004–5064.
7 B. E. Conway, Transition from "Supercapacitor" to "Battery" Behavior in Electrochemical Energy Storage, *J. Electrochem. Soc.*, 1991, **138**, 1539.
8 S. Fleischmann, J. B. Mitchell, R. Wang, C. Zhan, D.-e. Jiang, V. Presser and V. Augustyn, Pseudocapacitance: From Fundamental Understanding to High Power Energy Storage Materials, *Chem. Rev.*, 2020, **120**, 6738.
9 J. W. Darcy, B. Koronkiewicz, G. A. Parada and J. M. Mayer, A Continuum of Proton-Coupled Electron Transfer Reactivity, *Acc. Chem. Res.*, 2018, **51**, 2391.
10 J. L. Peper and J. M. Mayer, Manifesto on the Thermochemistry of Nanoscale Redox Reactions for Energy Conversion, *ACS Energy Lett.*, 2019, **4**, 866.
11 A. Ruiz Puigdollers, P. Schlexer, S. Tosoni and G. Pacchioni, Increasing Oxide Reducibility: The Role of Metal/Oxide Interfaces in the Formation of Oxygen Vacancies, *ACS Catal.*, 2017, **7**, 6493.
12 M. V. Ganduglia-Pirovano, A. Hofmann and J. Sauer, Oxygen vacancies in transition metal and rare earth oxides: Current state of understanding and remaining challenges, *Surf. Sci. Rep.*, 2007, **62**, 219.
13 R. G. Agarwal, H.-J. Kim and J. M. Mayer, Nanoparticle O–H Bond Dissociation Free Energies from Equilibrium Measurements of Cerium Oxide Colloids, *J. Am. Chem. Soc.*, 2021, **143**, 2896.
14 A. A. Fertig, W. W. Brennessel, J. R. McKone and E. M. Matson, Concerted Multiproton–Multielectron Transfer for the Reduction of O2 to H_2O with a Polyoxovanadate Cluster, *J. Am. Chem. Soc.*, 2021, **143**, 15756.
15 S. E. Cooney, A. A. Fertig, M. R. Buisch, W. W. Brennessel and E. M. Matson, Coordination-induced bond weakening of water at the surface of an oxygen-deficient polyoxovanadate cluster, *Chem. Sci.*, 2022, **13**, 12726.
16 E. Schreiber, A. A. Fertig, W. W. Brennessel and E. M. Matson, Oxygen-Atom Defect Formation in Polyoxovanadate Clusters via Proton-Coupled Electron Transfer, *J. Am. Chem. Soc.*, 2022, **144**, 5029.
17 S. Chakraborty, E. Schreiber, K. R. Sanchez-Lievanos, M. Tariq, W. W. Brennessel, K. E. Knowles and E. M. Matson, Modelling local structural and electronic consequences of proton and hydrogen-atom uptake in VO2 with polyoxovanadate clusters, *Chem. Sci.*, 2021, **12**, 12744.
18 E. Schreiber, W. W. Brennessel and E. Matson, Regioselectivity of Concerted Proton-Electron Transfer at the Surface of a Polyoxovanadate Cluster, *Chem. Sci.*, 2023, **14**, 1386.
19 S. Chakraborty, B. E. Petel, E. Schreiber and M. Ellen, Matson, Atomically precise vanadium-oxide clusters, *Nanoscale Adv.*, 2021, **3**, 1293.
20 A. A. Fertig and E. M. Matson, Connecting Thermodynamics and Kinetics of Proton Coupled Electron Transfer at Polyoxovanadate Surfaces Using the Marcus Cross Relation, *Inorg. Chem.*, 2023, **62**, 1958.
21 C. Baffert, S. W. Feldberg, A. M. Bond, D.-L. Long and L. Cronin, pH-Dependence of the aqueous electrochemistry of the two-electron reduced α-$[Mo_{18}O_{54}(SO_3)]$ sulfite Dawson-like polyoxometalate anion derived from its triethanolammonium salt, *Dalton Trans.*, 2007, 4599.
22 P. J. S. Richardt, R. W. Gable, A. M. Bond and A. G. Wedd, Synthesis and Redox Characterization of the Polyoxo Anion, γ*-$[S_2W_{18}O_{62}]^{4-}$: A Unique Fast Oxidation Pathway Determines the Characteristic Reversible Electrochemical Behavior of Polyoxometalate Anions in Acidic Media, *Inorg. Chem.*, 2001, **40**, 703.
23 S.-X. Guo, S. W. Feldberg, A. M. Bond, D. L. Callahan, P. J. S. Richardt and A. G. Wedd, Systematic Approach to the Quantitative Voltammetric Analysis of the FeIII/FeII Component of the $[\alpha_2\text{-}Fe(OH_2)P_2W_{17}O_{61}]^{7-/8-}$ Reduction Process in Buffered and Unbuffered Aqueous Media, *J. Phys. Chem. B*, 2005, **109**, 20641.
24 P. D. Prenzler, C. Boskovic, A. M. Bond and A. G. Wedd, Coupled Electron- and Proton-Transfer Processes in the Reduction of α-$[P_2W_{18}O_{62}]^{6-}$ and α-$[H_2W_{12}O_{40}]^{6-}$ As Revealed by Simulation of Cyclic Voltammograms, *Anal. Chem.*, 1999, **71**, 3650.
25 T. Ueda, K. Kodani, H. Ota, M. Shiro, S.-X. Guo, J. F. Boas and A. M. Bond, Voltammetric and Spectroscopic Studies of α- and β-$[PW_{12}O_{40}]^{3-}$ Polyoxometalates in Neutral and

Acidic Media: Structural Characterization as Their [(n-$Bu_4N)_3$][$PW_{12}O_{40}$] Salts, *Inorg. Chem.*, 2017, **56**, 3990.
26 S. Himeno, M. Takamoto, R. Santo and A. Ichimura, Redox Properties and Basicity of Keggin-Type Polyoxometalate Complexes, *Bull. Chem. Soc. Jpn.*, 2005, **78**, 95.
27 T. Ueda, J.-i. Nambu, J. Lu, S.-X. Guo, Q. Li, J. F. Boas, L. L. Martin and A. M. Bond, Structurally characterised vanadium(v)-substituted Keggin-type heteropolysulfates $[SVM_{11}O_{40}]^{3-}$ (M = Mo, W): voltammetric and spectroscopic studies related to the V(v)/V(iv) redox couple, *Dalton Trans.*, 2014, **43**, 5462.
28 V. W. Day, W. G. Klemperer and D. J. Maltbie, Where are the protons in $H_3V_{10}O_{28}{}^{3-}$?, *J. Am. Chem. Soc.*, 1987, **109**, 2991.
29 B. E. Petel, A. A. Fertig, M. L. Maiola, W. W. Brennessel and E. M. Matson, Controlling Metal-to-Oxygen Ratios via M=O Bond Cleavage in Polyoxovanadate Alkoxide Clusters, *Inorg. Chem.*, 2019, **58**, 10462.
30 R. G. Agarwal, S. C. Coste, B. D. Groff, A. M. Heuer, H. Noh, G. A. Parada, C. F. Wise, E. M. Nichols, J. J. Warren and J. M. Mayer, Free Energies of Proton-Coupled Electron Transfer Reagents and Their Applications, *Chem. Rev.*, 2022, **122**, 1.
31 C. Daniel and H. Hartl, Neutral and Cationic VIV/VV Mixed-Valence Alkoxo-polyoxovanadium Clusters $[V_6O_7(OR)_{12}]^{n+}$ (R = $-CH_3$, $-C_2H_5$): Structural, Cyclovoltammetric and IR-Spectroscopic Investigations on Mixed Valency in a Hexanuclear Core, *J. Am. Chem. Soc.*, 2005, **127**, 13978.
32 B. E. Petel, W. W. Brennessel and E. M. Matson, Oxygen-Atom Vacancy Formation at Polyoxovanadate Clusters: Homogeneous Models for Reducible Metal Oxides, *J. Am. Chem. Soc.*, 2018, **140**, 8424.
33 J. Spandl, C. Daniel, I. Brüdgam and H. Hartl, Synthesis and Structural Characterization of Redox-Active Dodecamethoxoheptaoxohexavanadium Clusters, *Angew. Chem., Int. Ed.*, 2003, **42**, 1163.
34 D. X. Ren, N. Xing, H. Shan, C. Chen, Y. Z. Cao and Y. H. Xing, Novel vanadium(iii) complexes with rigid phenylpolycarboxylate ligands: synthesis, structures and application in C–H bond activation, *Dalton Trans.*, 2013, **42**, 5379.
35 I. E. Grey, I. C. Madsen, K. Sirat and P. W. Smith, Structure of trans-diaquabis(oxalato)vanadate(III) complexes: A[V$(C_2O_4)_2(H_2O)_2$]•xH_2O, A = Cs (x = 4) and A = CH_3NH_3 (x = 4.5), *Acta Crystallogr., Sect. C: Cryst. Struct. Commun.*, 1985, **41**, 681.
36 C. J. Reed and T. Agapie, A Terminal Fe^{III}–Oxo in a Tetranuclear Cluster: Effects of Distal Metal Centers on Structure and Reactivity, *J. Am. Chem. Soc.*, 2019, **141**, 9479.
37 A. J. Ward, A. Ruseckas, M. M. Kareem, B. Ebenhoch, L. A. Serrano, M. Al-Eid, B. Fitzpatrick, V. M. Rotello, G. Cooke and I. D. W. Samuel, The Impact of Driving Force on Electron Transfer Rates in Photovoltaic Donor–Acceptor Blends, *Adv. Mater.*, 2015, **27**, 2496.
38 G. M. Loudon, *Organic Chemistry*, Roberts and Company, 2009.
39 F. G. Bordwell and M. J. Bausch, Acidity-oxidation-potential (AOP) values as estimates of relative bond dissociation energies and radical stabilities in dimethyl sulfoxide solution, *J. Am. Chem. Soc.*, 1986, **108**, 1979.
40 F. G. Bordwell, J. P. Cheng and J. A. Harrelson, Homolytic bond dissociation energies in solution from equilibrium acidity and electrochemical data, *J. Am. Chem. Soc.*, 1988, **110**, 1229.
41 J. J. Warren, T. A. Tronic and J. M. Mayer, Thermochemistry of Proton-Coupled Electron Transfer Reagents and its Implications, *Chem. Rev.*, 2010, **110**, 6961.
42 T. G. Carrell, P. F. Smith, J. Dennes and G. C. Dismukes, Entropy and enthalpy contributions to the kinetics of proton coupled electron transfer to the $Mn_4O_4(O_2PPh_2)_6$ cubane, *Phys. Chem. Chem. Phys.*, 2014, **16**, 11843.
43 N. Kindermann, C.-J. Günes, S. Dechert and F. Meyer, Hydrogen Atom Abstraction Thermodynamics of a μ-1,2-Superoxo Dicopper(ii) Complex, *J. Am. Chem. Soc.*, 2017, **139**, 9831.
44 E. Schreiber, W. W. Brennessel and E. M. Matson, Charge-State Dependence of Proton Uptake in Polyoxovanadate-alkoxide Clusters, *Inorg. Chem.*, 2022, **61**, 4789.
45 C. J. Fecenko, H. H. Thorp and T. J. Meyer, The Role of Free Energy Change in Coupled Electron–Proton Transfer, *J. Am. Chem. Soc.*, 2007, **129**, 15098.
46 M. Bourrez, R. Steinmetz, S. Ott, F. Gloaguen and L. Hammarström, Concerted proton-coupled electron transfer from a metal-hydride complex, *Nat. Chem.*, 2015, **7**, 140.
47 J. W. Darcy, S. S. Kolmar and J. M. Mayer, Transition State Asymmetry in C–H Bond Cleavage by Proton-Coupled Electron Transfer, *J. Am. Chem. Soc.*, 2019, **141**, 10777.
48 T. Huang, E. S. Rountree, A. P. Traywick, M. Bayoumi and J. L. Dempsey, Switching between Stepwise and Concerted Proton-Coupled Electron Transfer Pathways in Tungsten Hydride Activation, *J. Am. Chem. Soc.*, 2018, **140**, 14655.
49 S. K. Barman, J. R. Jones, C. Sun, E. A. Hill, J. W. Ziller and A. S. Borovik, Regulating the Basicity of Metal–Oxido Complexes with a Single Hydrogen Bond and Its Effect on C–H Bond Cleavage, *J. Am. Chem. Soc.*, 2019, **141**, 11142.
50 D. Usharani, D. C. Lacy, A. S. Borovik and S. Shaik, Dichotomous Hydrogen Atom Transfer vs Proton-Coupled Electron Transfer During Activation of X–H Bonds (X = C, N, O) by Nonheme Iron–Oxo Complexes of Variable Basicity, *J. Am. Chem. Soc.*, 2013, **135**, 17090.
51 M. K. Goetz and J. S. Anderson, Experimental Evidence for pKa-Driven Asynchronicity in C–H Activation by a Terminal Co(iii)–Oxo Complex, *J. Am. Chem. Soc.*, 2019, **141**, 4051.
52 S. K. Barman, M.-Y. Yang, T. H. Parsell, M. T. Green and A. S. Borovik, Semiempirical method for examining asynchronicity in metal–oxido-mediated C–H bond activation, *Proc. Natl. Acad. Sci. U. S. A.*, 2021, **118**, e2108648118.
53 J. E. Schneider, M. K. Goetz and J. S. Anderson, Statistical analysis of C–H activation by oxo complexes supports diverse thermodynamic control over reactivity, *Chem. Sci.*, 2021, **12**, 4173.

54 C. E. Elwell, M. Mandal, C. J. Bouchey, L. Que, Jr., C. J. Cramer and W. B. Tolman, Carboxylate Structural Effects on the Properties and Proton-Coupled Electron Transfer Reactivity of $[CuO_2CR]^{2+}$ Cores, *Inorg. Chem.*, 2019, **58**, 15872.
55 S. C. Coste, A. C. Brezny, B. Koronkiewicz and J. M. Mayer, C–H oxidation in fluorenyl benzoates does not proceed through a stepwise pathway: revisiting asynchronous proton-coupled electron transfer, *Chem. Sci.*, 2021, **12**, 13127.
56 E. R. Sayfutyarova, Y.-C. Lam and S. Hammes-Schiffer, Strategies for Enhancing the Rate Constant of C–H Bond Cleavage by Concerted Proton-Coupled Electron Transfer, *J. Am. Chem. Soc.*, 2019, **141**, 15183.
57 T. Yamakado, S. Takahashi, K. Watanabe, Y. Matsumoto, A. Osuka and S. Saito, Conformational Planarization versus Singlet Fission: Distinct Excited-State Dynamics of Cyclooctatetraene-Fused Acene Dimers, *Angew. Chem., Int. Ed.*, 2018, **57**, 5438.
58 J. Lee, K. Shizu, H. Tanaka, H. Nakanotani, T. Yasuda, H. Kaji and C. Adachi, Controlled emission colors and singlet–triplet energy gaps of dihydrophenazine-based thermally activated delayed fluorescence emitters, *J. Mater. Chem. C*, 2015, **3**, 2175.
59 *CrysAlisProf, version 171.41.97a*, Rigaku Corporation, Oxford, UK, 2021.
60 G. Sheldrick, SHELXT - Integrated space-group and crystal-structure determination, *Acta Crystallogr., Sect. A: Found. Adv.*, 2015, **71**, 3.
61 G. Sheldrick, Crystal structure refinement with SHELXL, *Acta Crystallogr., Sect. C: Struct. Chem.*, 2015, **71**, 3.